Original Article

Mitophagy and immune cell interaction: insights into pathogenesis and potential targets for necrotizing enterocolitis

Xinyun Jin[1,2], Wenqiang Sun[1,2], Yihui Li[1,2], Xueping Zhu[1]

[1]Department of Neonatology, Children's Hospital of Soochow University, Suzhou, China; [2]Clinical Pediatrics School, Soochow University, Suzhou, China

Contributions: (I) Conception and design: X Zhu, X Jin; (II) Administrative support: X Zhu; (III) Provision of study materials or patients: X Jin; (IV) Collection and assembly of data: W Sun, Y Li; (V) Data analysis and interpretation: X Jin, W Sun; (VI) Manuscript writing: All authors; (VII) Final approval of manuscript: All authors.

Correspondence to: Xueping Zhu, PhD. Department of Neonatology, Children's Hospital of Soochow University, No. 92, Zhongnan Street, Suzhou 215025, China. Email: zhuxueping4637@hotmail.com.

Background: Neonatal necrotizing enterocolitis (NEC) is a fatal disease in early life characterized by an inflammatory response or even necrosis of the bowel wall. NEC is one of the leading causes of preterm infant mortality. The pathogenesis of NEC is intricate and involves mitochondrial damage to intestinal cells and infiltration of immune cells. However, the specific functions of mitophagy and its association with immune cells in NEC remain unclear. The aim of this study was to explore the pivotal roles of mitophagy and the immune microenvironment in NEC and their potential interactions.

Methods: Microarray data (GSE46619) associated with NEC were obtained from the Gene Expression Omnibus (GEO) at the National Center for Biotechnology Information (NCBI). Differentially expressed genes (DEGs) were screened by GEO2R. Mitophagy gene data were downloaded from the Pathway Unification database and subjected to Gene Ontology (GO) and Kyoto Encyclopedia of Genes and Genomes (KEGG) pathway analyses. Consequently, mitophagy-related differentially expressed genes (MRDEGs) were obtained. To identify hub MRDEGs that are closely associated with NEC, we used CytoHubba, Molecular Complex Detection (MCODE) and Comparative Toxicogenomics Database (CTD) scores. Cytoscape and miRWalk databases were used to predict the transcription factors (TFs) and target microRNAs (miRNAs) of hub MRDEGs, respectively, and a regulatory network was established. The ImmuCellAI was used to analyze the pattern of immune infiltration, and the Spearman correlation was used to investigate the relationship between the hub MRDEGs and the abundance of infiltrating immune cells. Finally, the expression levels of the hub MRDEGs were verified by quantitative real-time polymerase chain reaction (qRT-PCR) and Western blotting in NEC animal model.

Results: A total of 14 up-regulated and 22 down-regulated MRDEGs were identified, these genes exhibited enrichment in mitophagy, and inflammation-related pathways. Furthermore, 13 hub MRDEGs closely related to NEC were identified. The increased presence of immune cells such as neutrophils, M1 macrophages, and activated mast cells were observed while adaptive immune cells including B cells and various T-cell subsets exhibited reduced infiltration. Furthermore, up-regulated MRDEGs were positively correlated with the proinflammatory immune cell infiltration, and the down-regulated MRDEGs were positively correlated with the anti-inflammatory immune cell infiltration. *In vivo* experiments demonstrated that the expressions of four genes *Hif-1a*, *Acsl4*, *Pck2*, and *Aifm1* were consistent with the bioinformatics analysis results.

Conclusions: The potential interplay of mitophagy and immune cells is crucial in the onset and progression of NEC. This perspective opens the door for deeper investigations into NEC pathogenesis, presenting a possible target for disease intervention.

Keywords: Necrotizing enterocolitis (NEC); mitophagy; immune infiltration; bioinformatics analysis

Submitted Oct 17, 2024. Accepted for publication Jan 21, 2025. Published online Feb 25, 2025.
doi: 10.21037/tp-24-441
View this article at: https://dx.doi.org/10.21037/tp-24-441

Introduction

Background

Necrotizing enterocolitis (NEC) is one of the most lethal gastrointestinal disorders in preterm infants that mainly affects low birth weight infants. Low birth weight (<2,500 g) and very low birth weight (≤1,500 g) infants have a 1.2% and 2.5% prevalence of NEC, respectively (1). Although preterm infants' survival and long-term outcomes have improved, the NEC-related mortality rate continues to increase at approximately 20–40% (2). However, 25–50% of NEC patients are surgically treated, and survivors frequently suffer from intestinal stenosis, short bowel syndrome (SBS), and neurodevelopmental deficits (3). Since preventive strategies and treatment options for NEC are limited, there is an urgent need to explore the pathogenesis of NEC and find novel targeted therapeutic options.

Mitochondria are key organelles that control cellular fate and metabolism, stress responses, and cell death. Numerous inflammatory bowel conditions have been associated with mitochondrial dysfunction and inflammatory immune response (4,5). There is increasing evidence that NEC etiology involves mitochondrial dysfunction (6,7). A study showed that mitochondria are central to the immune response and can facilitate the transduction of signals for numerous innate immune responses; however, in pathological conditions, mitochondria can be a source of damage associated molecular patterns (DAMPs) (8). They also play a major role in the immune metabolism by alternating between oxidative phosphorylation and glycolysis, which influences the cellular activation of the macrophages, dendritic cells, T cells, and other cells. Glycolysis dominates in the pro-inflammatory classical activation of macrophages, whereas oxidative phosphorylation is predominant in tissue repair. Inhibition of intrinsic macrophage mammalian target of rapamycin (mTOR) and glycolysis promotes oxidative phosphorylation, induces mitophagy to cull dysfunctional mitochondria, and reduces the inflammatory stimuli of mitochondrial DAMPs. By acting as a mitochondrial quality control mechanism, mitophagy maintains the internal environment's stability by selectively removing dysfunctional mitochondria (9) and hence might be closely related to the pathogenesis of NEC. Nonetheless, in the absence of mitophagy, mitochondrial DAMPs lead to hyperinflammation and subsequent pathological changes.

To conclude, adequate mitophagy is essential for balancing the innate immune response to inflammation. Using various microarray data levels, bioinformatics enables the screening of molecules to extract the differences between patients and healthy individuals. Hence, it can be effective for exploring the underlying molecular mechanisms of NEC. Thus, we analyzed how mitophagy-related genes (MRGs) contribute to the development of NEC and influence immune infiltration based on the Gene Expression Omnibus (GEO) database (GSE46619) microarray data. To better understand the underlying pathological mechanisms during disease development, we investigated the relationship between hub MRGs and immune infiltration in NEC. To further validate our findings, we examined the expression of these MRGs in the neonatal mouse model of NEC, providing additional insights into their role in the disease pathogenesis. We present this article in accordance with the ARRIVE reporting checklist (available at https://tp.amegroups.com/article/view/10.21037/tp-24-441/rc).

Highlight box

Key findings

- Mitophagy-related genes might induce or inhibit the development of necrotizing enterocolitis (NEC) by regulating immune cell infiltration. Targeting *HIF1A*, *ACSL4*, *PCK2*, and *AIFM1* genes might improve the abnormal immune status in NEC.

What is known and what is new?

- The pathogenesis of NEC is intricate and involves mitochondrial damage to intestinal cells and infiltration of immune cells.
- The specific functions of mitophagy and its association with immune cells in NEC remain unclear.

What is the implication, and what should change now?

- In our study, the expression of mitophagy-related genes in NEC and their possible interactions with the immune microenvironment were identified for the first time using bioinformatics. HIF-1α, ACSL4, PCK2, and AIFM1 were screened and validated to provide potential molecular targets for in-depth investigation of NEC pathogenesis.

Methods

Microarray data retrieval

The NEC datasets were downloaded from the GEO database at the National Center for Biotechnology Information (NCBI) using the search term "necrotizing enterocolitis". These datasets were further screened based on characteristics such as sequencing type (transcriptology), animal species (humans, Homo sapiens), and sample source (bowels). This selection ensured that the obtained dataset comprised NEC-related gene expression profiles that originated from human intestinal tissues. Finally, the GSE46619 dataset was obtained. The GSE46619 [(HuGene-1_0-st) Affymetrix Human Gene 1.0 ST Array] dataset is generated by the GPL6244 platform that contains 14 bowel tissues of patients and includes 5 samples of NEC, 4 samples of Surgical-Control as well as 5 samples of spontaneous intestinal perforations (SIP), respectively. The Surgical-Control samples were derived from patients with congenital intestinal malformations that were non-inflammatory, as identified in the original dataset. Finally, we collected nine samples of patients, including 5 NEC and 4 surgical-control samples to analyze the differential genes between the NEC and surgical-control (Control) groups.

Microarray data acquisition and identification of differentially expressed genes (DEGs)

R package "GEO query" was used to access microarray data from GEO. The R package "limma" was used to retrieve DEGs from each microarray. All identified DEGs met $P<0.05$ and $|\log_2 \text{fold change (FC)}| \geq 1$. With "ggplot2", volcano plot was used to visualize the DEGs.

Identification of mitophagy-related DEGs (MRDEGs)

The Pathway Unification database, was visited to obtain MRGs. With a Venn Diagram, the DEGs from the microarray and the 772 MRGs were intersected to identify MRDEGs. The R package "ggplot2" was then used to visualize as Heatmap and Boxplot.

Gene enrichment analysis

Using clusterProfiler, MRDEGs were analyzed for Gene Ontology (GO) and Kyoto Encyclopedia of Genes and Genomes (KEGG) pathway enrichment. All values of $P<0.05$ in the Benjamini-Hochberg test were deemed statistically significant. Finally, Bar graphs and Circle graphs were generated by using R packages "ggplot2" and "GOplot", respectively.

Analysis of protein-protein interaction (PPI) and acquisition of crucial NEC-related genes

The MRDEGs were processed for PPI analysis with the STRING database; Cytoscape 3.9.1 was used to visualize the resulting interactions. Additionally, using the plug-ins CytoHubba and Molecular Complex Detection (MCODE) implemented by Cytoscape 3.9.1 to filter out hub MRDEGs.

The Comparative Toxicogenomics Database (CTD) assembled interaction data between genes, products, functional phenotypes, and diseases. These data facilitated research into potential therapeutic modes of action. The CTD data helped in analyzing the risk of NEC development in relation to hub MRDEGs.

Prediction of a transcription factors (TFs)-microRNAs (miRNAs)-hub MRDEGs network

To identify the upstream regulators of hub MRDEGs, TFs of hub MRDEGs were used to explore with the iRegulon plug-in of Cytoscape 3.9.1. Furthermore, the miRWalk database was used to project the miRNAs of hub MRDEGs. Networks of TFs and miRNAs was visualized using Cytoscape 3.9.1.

Analysis of immune infiltration

Using the CIBERSORT algorithm, we determined the differences in the proportions of 22 types of immunocytes between the NEC and Control groups, respectively. "Vioplot" and "GOplot" were used to visualize the results. The corrplot package was used for drawing the correlation heatmap. Spearman correlation analysis helped in exploring the link between hub MRDEGs and the immune cells by using the "psych" and "reshape2" packages while the "heatmap" package was used to visualize the results.

Construction of animal models

Experiments were performed under a project license (No. SUDA20240108A01) granted by the Ethics Committee of Soochow University, in compliance with the Ethics Committee of Soochow University institutional guidelines for the care and use of animals. Six-day-old C57BL/6

Table 1 The primers used in this study

Gene	Forward sequence (5' to 3')	Reverse sequence (5' to 3')
Pdk2	TGGACCGCTTCTACCTCAG	TCTTTCACCACATCAGACACG
Tspo	GCCTACTTTGTACGTGGCGAG	CCTCCCAGCTCTTTCCAGAC
Gls	GACAACGTCAGATGGTGTCAT	TGCTTGTGTCAACAAAACAATGT
Acsl4	TCCTCCAAGTAGACCAACCCC	AGTCCAGGGATACGTTCACAC
Aifm1	CTGGATGTAAGAGGCAACATGG	CCGCCGATAACTGTAATTGACT
Pck2	GTGGCCGTGCAATCCAGAA	GATGCCCAAAATCAGCATGTG
Ppargc1α	AGACGGATTGCCCTCATTTGA	GGTCTTAACAATGGCAGGGTTT
Sdha	GAACACTCCAAAAACAGACCTGC	TCCACCACTGGGTATTGAGTAG
Tfrc	GTTTCTGCCAGCCCCTTATTAT	GCAAGGAAAGGATATGCAGCA
Hk2	GTGTGCTCCGAGTAAGGGTG	CAGGCATTCGGCAATGTGG
Glul	CTGAGTGGAACTTTGATGGCT	GGAAGGGGTCTCGAAACATGG
Gfpt2	AGCAAAGGCTACGAGTTTGAG	GACTCTTTCGACCAATGTGGAA
Hif1α	TCTCGGCGAAGCAAAGAGTC	AGCCATCTAGGGCTTTCAGATAA
Actin	AGAGGGAAATCGTGCGTGAC	CAATAGTGATGACCTGGCCGT

neonatal male mice were bought from JOINN Laboratories [Suzhou, China, License No. SCXK (Su) 2019-0004]. The 6-day-old C57BL/6 mice model of NEC was induced according to previous protocols with some modifications (10,11). The neonatal mice were randomly divided into the NEC (10 mice) and the Control (5 mice) groups, respectively. The NEC group's modeling conditions were: (I) the mice were exposed to a hypoxic environment (95% N_2 + 5% O_2) at a fixed time twice a day for 10 min; (II) the mice were tube-fed hypertonic formula milk once every 3 hours at a dose of 40 μL/g as per their body weight; (III) they were subjected to low-temperature (4 ℃) stimulation twice daily for 10 min, and (IV) lipopolysaccharides (LPS; Sigma, St. Louis, USA, 4 μg/g) was added into the second artificially fed formula on days 2–4 of modeling. The Control group was fed by the mothers without any intervention. The entire modeling cycle lasted 96 h.

All mice that reached the modeling endpoint were euthanized. Isoflurane at a concentration of 3% was used in this study to induce anaesthesia, resulting in rapid unconsciousness of the mice. Then the concentration of isoflurane was increased to 5% to bring the mice to a state of deep anaesthesia. To prevent resuscitation, the mice were immediately subjected to decapitation, using scissors to quickly sever the medulla oblongata to rapidly separate the head from the body. Furthermore, intestinal tissues were retained from the NEC (5 mice) and the Control (5 mice) groups, respectively.

Hematoxylin-eosin (HE) staining

Fresh terminal ileum was taken and put into paraformaldehyde solution for fixation, embedded in paraffin, sectioned by slicer to produce 5 μm paraffin sections. Slides were stained with HE. Scoring of the pathology was carried out independently by two pathologists with reference to the scoring criteria of Michael Caplan (12) (double blind method).

The extraction of RNA and quantitative real-time polymerase chain reaction (qRT-PCR)

Total RNA of intestinal tissues was extracted with Trizol (Novogene, Beijing, China). Subsequently, the total RNA was reverse transcribed into cDNA with the Reverse Transcription Kit (ABM, Richmond, Canada), followed by qRT-PCR using SYBR Green (Accurate Biology, Changsha, China). Each primer sequence was analyzed using the NCBI BLAST tool to confirm its specificity. Melting curve analysis was performed after each qPCR reaction to ensure the specific amplification. As shown in *Table 1*, the primers are used for amplification. The expression of target gene relative to the β-actin gene was demonstrated as $2^{-\Delta\Delta Ct}$.

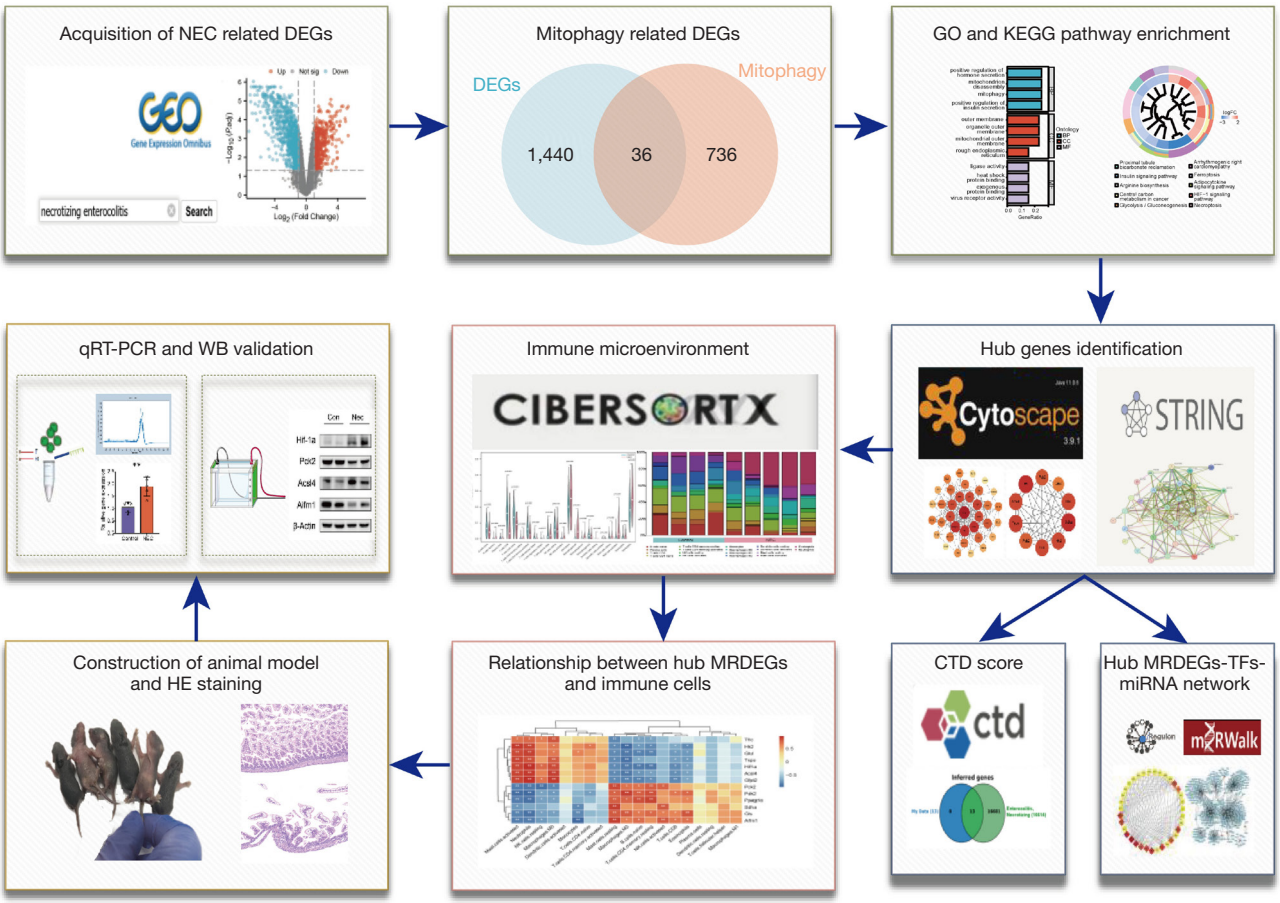

Figure 1 Study flow chart. NEC, necrotizing enterocolitis; DEGs, differentially expressed genes; GO, Gene Ontology; KEGG, Kyoto Encyclopedia of Genes and Genomes; BP, biological process; CC, cellular component; MF, molecular function; FC, fold change; qRT-PCR, quantitative real-time polymerase chain reaction; WB, Western blotting; HE, hematoxylin-eosin; MRDEGs, mitophagy-related differentially expressed genes; CTD, Comparative Toxicogenomics Database; TF, transcription factor; miRNA, microRNA.

Western blotting

The samples were retrieved from the ileal tissue and boiled in a loading buffer for ten minutes, followed by the administration of 10% sodium dodecyl sulfate-polyacrylamide gel electrophoresis (SDS-PAGE) for protein separation. PVDF membranes were incubated at 4 ℃ overnight with primary antibodies. The primary antibodies were: β-Actin (dilution 1:10,000, fd0060–100, Fude, Hangzhou, China), HIF-1α (dilution 1:100, sc-13515, Santa, Dallas, USA), ACSL4 (dilution 1:2,000, 22401–1-AP, ProteinTech, Wuhan, China), PCK2 (dilution 1:1,000, ab181170, Abcam, Cambridge, UK), and AIFM1 (dilution 1:2,000, ab32516, Abcam). Incubated with the secondary antibody at room temperature for 1 hour, the membranes were then detected with an electrochemiluminescence (ECL) system.

Statistical analysis

The mean ± standard deviation (SD) of three independent experiments was calculated using GraphPad Prism 8.0 (GraphPad Inc., San Diego, USA). The Shapiro-Wilk test was used to analyze the normality of the data. Additionally, normally distributed data were compared using the Student's *t*-test. It was considered statistically significant when the P value was less than 0.05.

Results

The DEGs in NEC and recognition of MRDEGs

The study flow chart is presented in *Figure 1*. The NEC-related GEO dataset, GSE46619 was obtained for analysis.

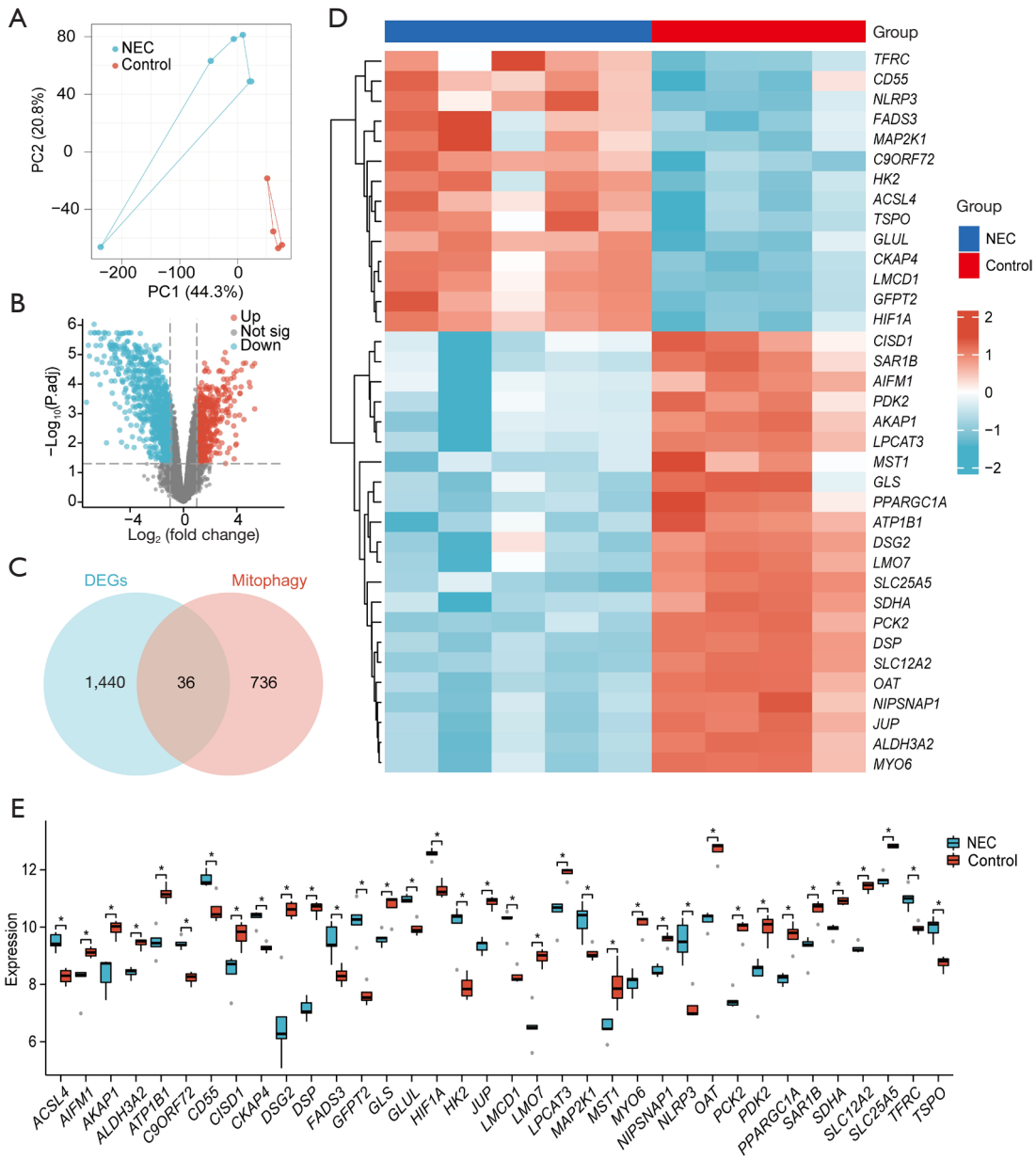

Figure 2 Differential gene analysis and identification of MRDEGs. (A) The PCA diagram of GSE46619; (B) volcano plot displaying significant DEGs in GSE46619; (C) Venn diagram showing the MRDEGs; (D) clustered heatmap of MRDEGs in bowel between Control and NEC groups; (E) comparison boxplot demonstrating the expression of 36 MRDEGs. *, P<0.05. NEC, necrotizing enterocolitis; PC, principal component; DEGs, differentially expressed genes; MRDEGs, mitophagy-related differentially expressed genes; PCA, principal component analysis.

According to the differential analysis of this dataset, there were 1,440 DEGs in the NEC group compared to the Control group, including 515 up-regulated genes and 925 down-regulated genes, respectively (*Figure 2A-2C*).

GeneCards were used to retrieve MRGs, and the MRDEGs were selected from the DEGs that overlapped with the MRGs (*Figure 2D,2E*). A total of 36 MRDEGs were obtained, including 14 up-regulated genes and 22 down-regulated genes in the NEC group when compared to the Control group.

Functional enrichment analysis of MRDEGs

The MRDEGs were functionally enriched using GO and KEGG pathway analysis. The most enriched up-regulated genes of GO terms were classified as biological process (BP), cellular component (CC), and molecular function (MF), with a focus on mitochondrial quality controls, mitochondrial outer membrane, rough endoplasmic reticulum, ligase activity and heat shock protein binding, etc. (*Figure 3A*). According to *Figure 3B*, the most enriched down-regulated genes of GO terms were associated with cell communication involved in cardiac conduction, cell-cell contact zone, active ion transmembrane transporter activity, and cell-cell adhesion mediator activity.

The KEGG pathways involved in numerous metabolic processes, hypoxia, and several regulating programmed cell deaths were the most enriched ones among the MRDEGs (*Figure 3C*).

Analysis of PPI networks and identification of hub MRDEGs

STRING database was used to analyze the PPI network of 36 MRDEGs and Cytoscape was used to visualize the network (*Figure 3D*). Additionally, by using the Cytoscape MCODE plug-in (degree cut-off =2, node score cut-off =0.2, K-core =2, and max depth =100), significant modules were identified. The module composed of 10 nodes and 37 edges involved the following genes: *SDHA*, *GLUL*, *GFPT2*, *PCK2*, *TFRC*, *ACSL4*, *TSPO*, *PDK2*, *GLS*, and *HK2* (*Figure 3E*). With the degree algorithm of CytoHubba plug-in, the PPI network helped in retrieving 10 hub genes including *HIF1A*, *SDHA*, *PPARGC1A*, *TFRC*, *TSPO*, *ACSL4*, *GLUL*, *GLS*, *HK2*, and *AIFM1* (*Figure 3F*). Moreover, using the PPI network, 10 hub genes were identified, including *HIF1A*, *PPARGC1A*, *SDHA*, *PDK2*, *GLS*, *PCK2*, *HK2*, *GLUL*, *GFPT2*, and *ACSL4* by using the maximum clique centrality (MCC) algorithm of CytoHubba plug-in (*Figure 3G*). Finally, a concatenation of the three algorithms was obtained, including *HIF1A*, *PPAGRC1A*, *SDHA*, *PDK2*, *GLS*, *PCK2*, *HK2*, *GLUL*, *GFPT2*, *ACSL4*, *TFRC*, *TSPO*, and *AIFM1* to investigate gene expression changes in NEC and their possible involvement in NEC pathophysiology.

Relationship between hub MRDEGs and NEC

In order to predict the relationship between hub MRDEG and NEC, the CTD database was used. Although, all 13 hub genes were associated with NEC (*Figure 4A*). *GLUL*, *GFPT2*, and *HIF1A* displayed the maximum association with NEC (*Figure 4B*). Additionally, approximately all hub MRDEGs were strongly correlated with inflammation and necrosis (Table S1).

TFs-miRNAs-Hub MRDEGs regulatory network

Predictions of miRNAs and TFs related to hub MRDEGs were conducted to explore upstream regulation. With Cytoscape's iRegulon plug-in, the TFs of hub MitoDEGs were predicted, and a hub MRDEGs-TFs regulatory network comprising 22 TFs (*NFYA*, *NFYB*, *NFYC*, *YBX1*, *POLE3*, *POLE4*, *HNF4A*, *NR2F1*, *NR2F2*, *RXRA*, *HNF4G*, *PPARA*, *PPARD*, *PPARG*, *NR2F6*, *ESRRA*, *NR2C2*, *NR1H2*, *RXRG*, *RXRB*, *CSTF2*, and *ESCAN10*) was constructed (*Figure 4C*). Moreover, using miRWalk 3.0, hub MRDEG-miRNA regulatory networks with 394 nodes and 1,016 edges were created (*Figure 4D*). Hsa-miR-6124 displayed interactions with *PPARGC1*A, *GLS*, and *TFRC*.

Immune cell infiltration in NEC

To investigate whether the MRDEG expression levels were correlated with immune cells, the CIBERSORT algorithm was used to analyze the infiltration of 22 immune cell types. The percentages of various immune cells were calculated using the par function and stacked histograms were subsequently plotted. Twelve immune cell types showed significant differences in intestinal infiltration between the Control and NEC groups ($P<0.05$). Specifically, neutrophils, activated mast cells, M0 macrophages, M1 macrophages, monocytes, and eosinophils were more abundant in the NEC group, while naïve B cells, $CD8^+$ T cells, naïve $CD4^+$ T cells, memory-activated $CD4^+$ T cells, plasma cells, and M2 macrophages were more abundant in the Control group (*Figure 5A-5C*). Further analysis of the infiltrating immune cells in the NEC group revealed multiple correlations (*Figure 5D*). The correlation degree was indicated by scores. The strongest synergistic effect was observed between naïve $CD4^+$ T cells and activated mast cells (0.96), followed by activated NK cells and resting mast cells (0.95) as well as M2 macrophages, and resting memory $CD4^+$ T cells (0.85), respectively. In contrast, the strongest competitive effect was observed between naïve $CD4^+$ T cells and resting memory $CD4^+$ T cells (–0.92), followed by activated mast cells and resting memory $CD4^+$ T cells (–0.91) as well as $CD8^+$ T cells and neutrophils (–0.87), activated mast cells and M2 macrophages.

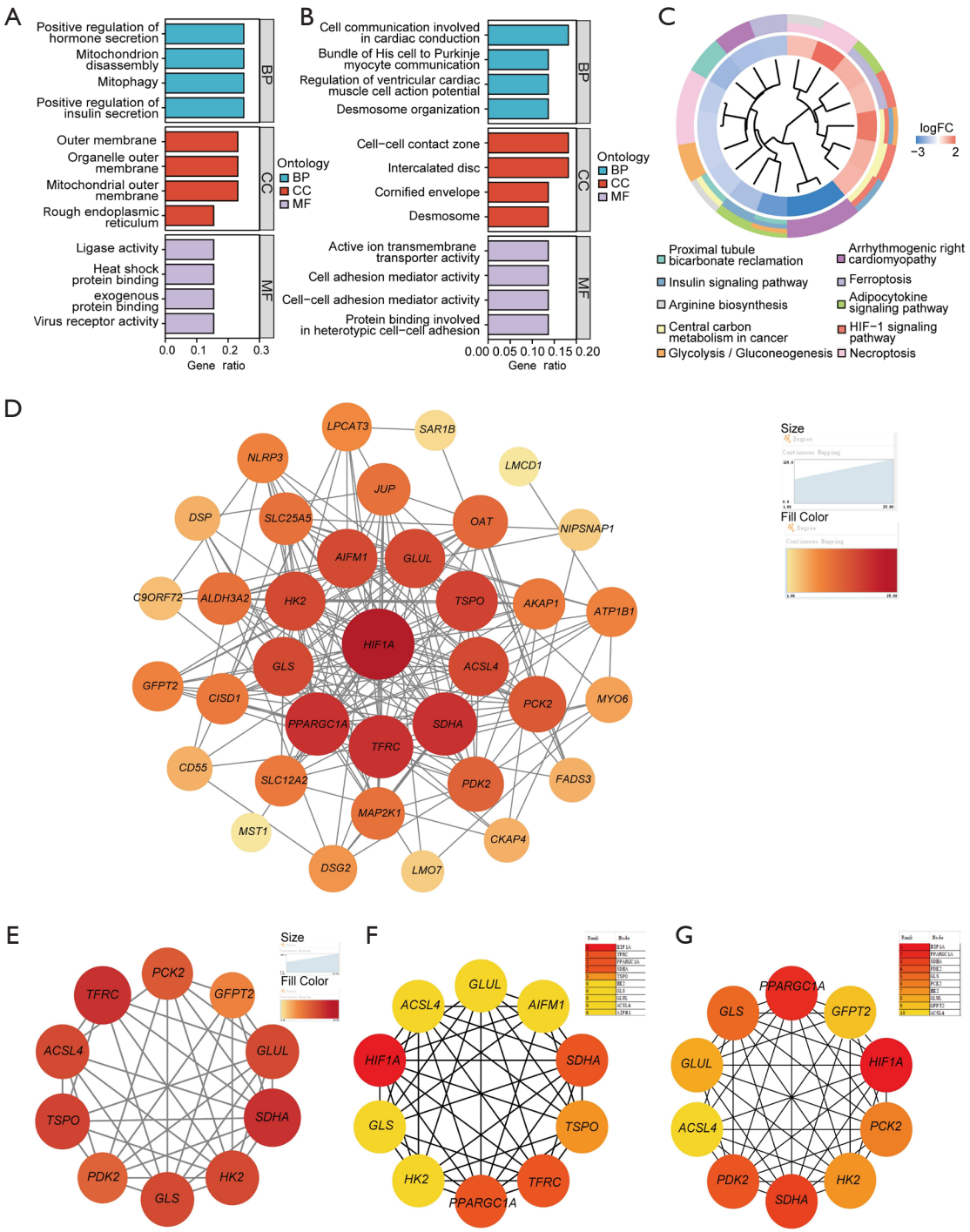

Figure 3 Functional enrichment analysis of MRDEGs and hub MRDEGs identification. (A,B) Barplot of GO enrichment analysis of up-regulated and down-regulated MRDEGs in BP, CC, and MF; (C) circle chart of KEGG pathway enrichment analysis of MRDEGs; (D) PPI network of MRDEGs: circle color and size representing the node degree; (E) an MRDEGs cluster was obtained using the MCODE plug-ins; (F,G) the top 10 hub genes separately selected by the degree and MCC algorithm separately of plug-in CytoHubba. BP, biological process; CC, cellular component; MF, molecular function; FC, fold change; MRDEGs, mitophagy-related differentially expressed genes; GO, Gene Ontology; KEGG, Kyoto Encyclopedia of Genes and Genomes; PPI, protein-protein interaction; MCODE, Molecular Complex Detection; MCC, maximum clique centrality.

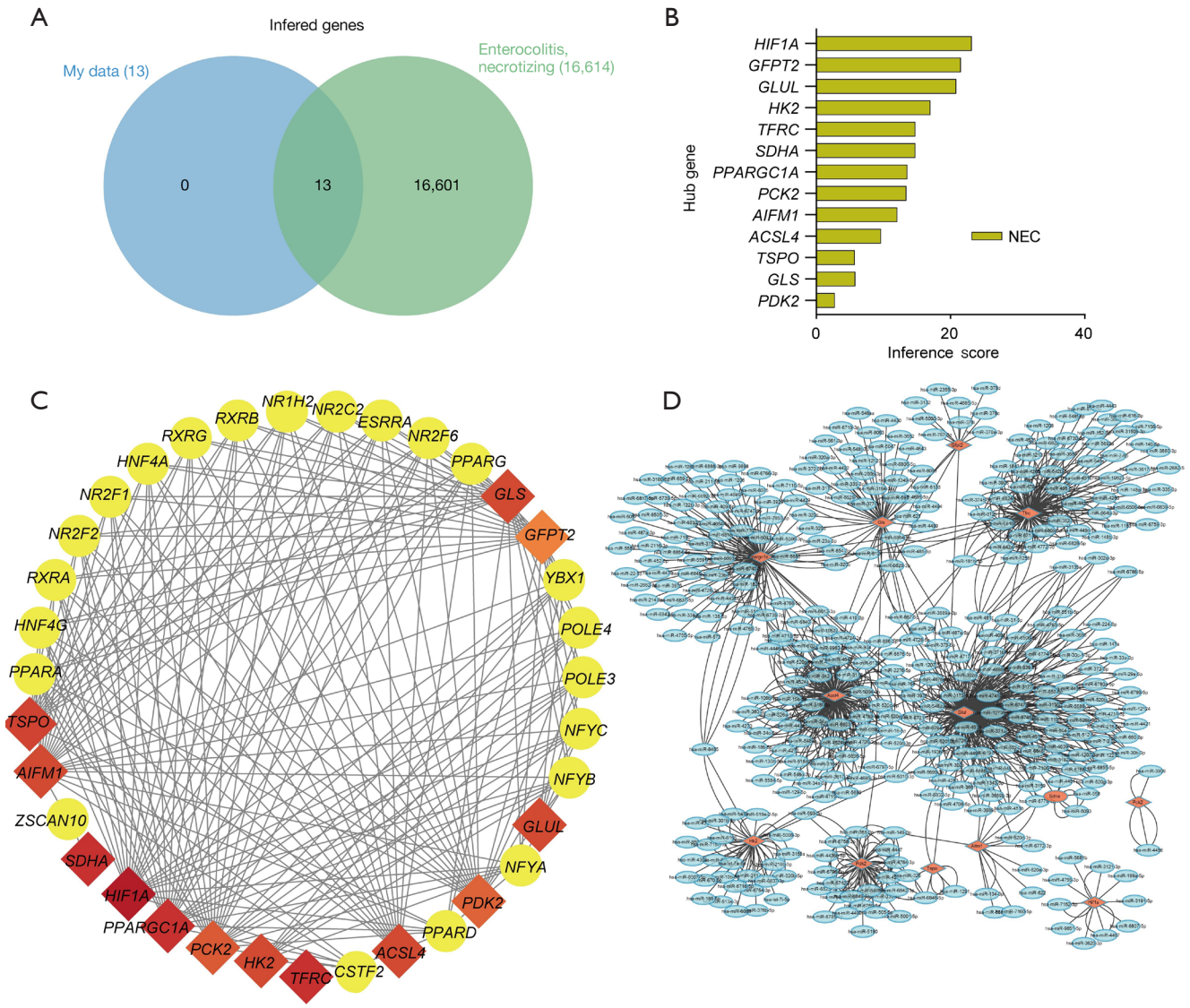

Figure 4 Relationship between hub MRDEGs and NEC; construction of TFs-miRNAs-hub MRDEGs regulating network. (A) Venn diagram illustrating the inferred genes identified as potentially involved in NEC development based on their evaluation through the CTD platform. (B) Barplot showing the inference scores, which indicate the strength of the association between hub MRDEGs and NEC, derived from the CTD platform. (C) TFs-hub MRDEGs regulatory network: the red nodes indicating hub MRDEGs, and the yellow nodes indicating TFs. (D) MiRNA-MRDEGs regulatory network: the red nodes indicating hub MRDEGs targeted by miRNAs, and the blue nodes indicating miRNAs. NEC, necrotizing enterocolitis; MRDEGs, mitophagy-related differentially expressed genes; TF, transcription factor; miRNA, microRNA; CTD, Comparative Toxicogenomics Database.

Relationship between hub MRDEGs and immune cells

Hub MRDEGs and immune cells were explored using the Spearman method. Of the 13 hub MRDEGs, genes like *HK2*, *GLUL*, *TSPO*, *HIF1A*, *ACSL4*, and *GFPT2* were positively associated with activated mast cells and neutrophils while *PCK2*, *PDK2*, *PPARGC1A*, *GLS*, and *AIFM1* were negatively associated with mast cells and Neutrophils. Although *TFRC* was negatively related with resting mast cells, *PCK2*, *PDK2*, *PPARGC1A*, *GLS*, and *AIFM1* showed positive correlations with resting mast cells. While resting NK cells showed a negative correlation with *PCK2*, activated NK cells were positively correlated

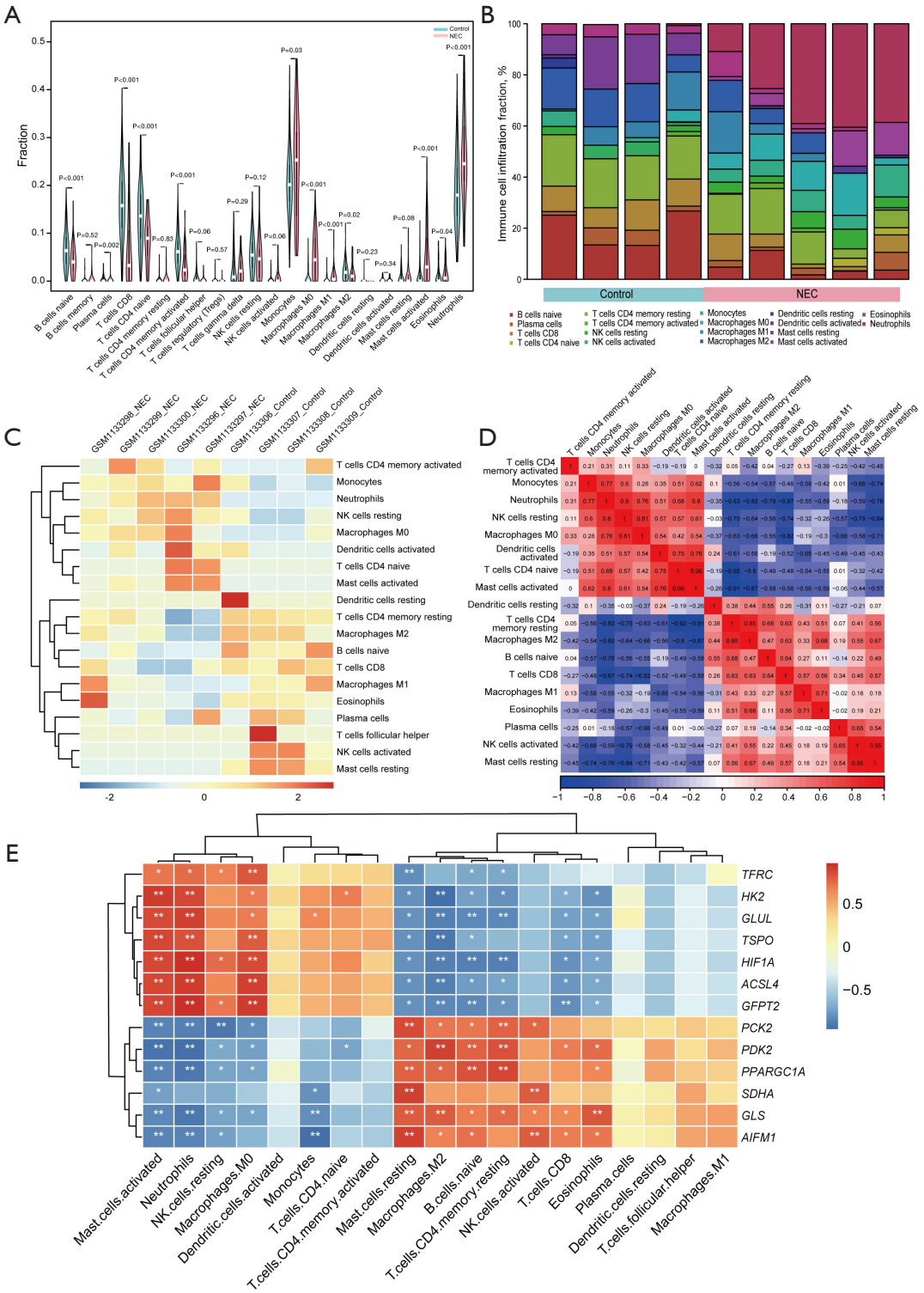

Figure 5 Landscape and correlation of immune cell infiltration and hub MRDEGs compared between the Control and NEC groups. (A,B) Violin plot and stacked histograms of differential infiltrating fractions. (C) Heatmap of immune cell expression in the data set. (D) The co-expression pattern among different immune cells. (E) The correlation between the hub MRDEGs and immune cells. *, P<0.05; **, P<0.01. NEC, necrotizing enterocolitis; MRDEGs, mitophagy-related differentially expressed genes.

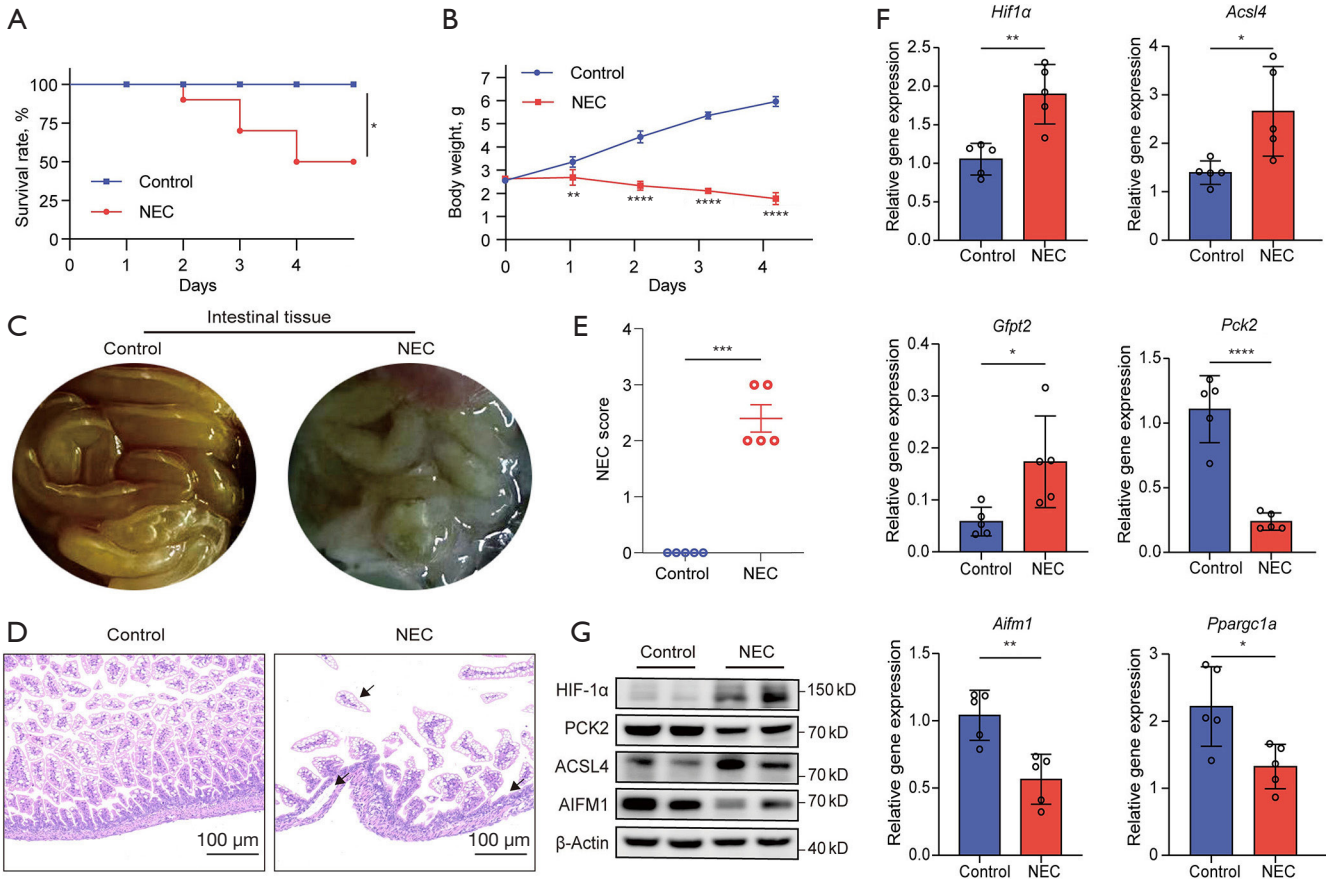

Figure 6 Validation of hub MRDEGs in NEC pups. (A) Survival rate of the two groups (n=10 in NEC group; n=5 in Control group). (B) Body weight changes of surviving pups in each group (n=5 per group). (C) Gross morphology of the two groups. (D) HE staining of bowel tissues. The arrows point to villus failed off, severe separation of submucosa and damaged crypt structure. (E) NEC pathogenic score of the two groups (n=5 per group). (F) The mRNA expression levels of 6 hub MRDEGs in two groups. (G) Representative Western blotting picture showing the expression of HIF-1α, ACSL4, PCK2 and AIFM1. *, P<0.05; **, P<0.01; ***, P<0.001; ****, P<0.0001. NEC, necrotizing enterocolitis; MRDEGs, mitophagy-related differentially expressed genes; HE, hematoxylin-eosin.

with *SDHA* and *AIFM1*. Moreover, *TFRC*, *TSPO*, *HIF1A*, *ACSL4*, and *GFPT2* were positively associated with M0 macrophages. *HK2*, *GLUL*, *TSPO*, *HIF1A*, *ACSL4*, and *GFPT2* as well as *PDK2* and *GLS* were negatively and positively associated with M2 macrophages, respectively. *GLS* and *AIFM1* showed negative correlations with monocytes. Additionally, *PDK2* and *PPARGC1A* as well as *GLUL*, *HIF1A*, and *GFPT2* were positively and negatively associated with naïve B cells, respectively. *PCK2*, *PDK2*, and *PPAGRC1A* were positively associated with resting memory CD4$^+$ T cells, but *GLUL* and *HIF1A* were positively associated with resting memory CD4$^+$ T cells. *GFPT2* was negatively associated with CD8$^+$ T cells, while *GLS* was positively related to eosinophils (*Figure 5E*).

Experimental validations of hub MRDEGs expression in NEC mice

Compared with those in the Control group, the biological features of the NEC pups were different. Survival rates in the NEC group were 50% while in the Control group they were 100%. Survival analyses showed that there was a difference in the NEC group compared to the Control group (P<0.05, *Figure 6A*). The neonatal pups in the NEC model group exhibited large degrees of growth retardation during the modeling process compared the Control group (*Figure 6B*). The small intestines of the Control pups were pale yellow, glossy and elastic when touched while those of the NEC pups were dark and black in colour, obviously brittle when touched, and ascites was visible (*Figure 6C*).

The intestinal tissue from the Control pups was structurally intact, while in the NEC pups' sections, the breakage and detachment of intestinal villi, separation of mucosal and lamina propria, and damaged crypt structure were observed (*Figure 6D*). Pathological scores suggested a statistically significant difference between the two groups (P<0.001, *Figure 6E*). The expression of 13 hub MRDEGs in intestinal tissue was validated by qRT-PCR. As compared to the Control pups, *Hif1a*, *Acsl4*, and *Gfpt2* showed significantly enhanced expression in the NEC pups (P<0.05), while *Pck2*, *Aifm1*, and *Ppargc1α* reversely exhibited decreased expressions in the NEC pups (P<0.05, *Figure 6F*). Additionally, we validated the protein expressions of HIF-1α, ACSL4, GFPT2, PCK2, AIFM1, and PPARGC1A within the two groups by Western blotting. In agreement with the mRNA results, protein expression levels of HIF-1α, ACSL4, PCK2, and AIFM1 were observed (*Figure 6G*).

Discussion

The occurrence of NEC can be life-threatening and cause neurological damage, particularly in extremely low birth weight infants (ELBWI) (2,3). Given the complexity of its pathogenesis, specific therapeutic interventions for NEC have not yet been established. Management primarily relies on supportive care, including nutritional support, antibiotics, and gastrointestinal decompression. Surgical intervention may be necessary in severe cases to remove necrotic tissue. Mitochondrial dysfunction plays a pivotal role in acute enteritis (13-15). Oxidative stress in NEC intestinal cells increases the production of mitochondrial intracellular reactive oxygen species (ROS) and activates the mitochondrial apoptotic signaling pathway (16). Additionally, injury in NEC intestine enhances the release of mitochondrial deoxyribonucleic acid (mtDNA) from the intestinal tract into the circulation (17). NEC-associated intestinal injury can be reduced by modulating mitochondrial damage in intestinal epithelial cells and inhibiting mast cell accumulation in the ileal tissue of NEC rats (18). Mitophagy, a mitochondrial quality control mechanism, is activated in response to hypoxia and metabolic stress and maintains the stability of the internal environment by selectively removing dysfunctional mitochondria (9). This ensures that the mitochondria provide a normal signaling platform for pathogen-associated molecular patterns (PAMPs), and appropriately activate numerous immune responses. Therefore, this study used multiple bioinformatics methods to focus on the pathogenesis of NEC from the perspective of mitophagy to explore potential therapeutic targets.

The present study involved the extraction of DEGs from the NEC-related microarray dataset in GEO, followed by the application of MRGs from The Pathway Unification database. Subsequently, 36 MRDEGs were identified; the GO and KEGG enrichment analyses showed the presence of several mitophagy-related enrichment terms. Furthermore, C57 pups underwent NEC modeling for validation. Six genes (*Pck2*, *Hif1a*, *Acsl4*, *Aifm1*, *Gfpt2*, and *Ppargc1α*) showed PCR expression trends consistent with previous bioinformatics analyses. Additional validation revealed that the protein expressions of HIF-1α and ACSL4 as well as PCK2 and AIFM1 were up-regulated and down-regulated in NEC mice intestines, respectively.

Multiple activities of immune cells are closely related to the development of NEC. We further analysed various types of immune cell infiltration in the Control and NEC groups, respectively. Subsequently, we found the infiltration of some immune cells like neutrophils, monocytes, M1 macrophages, activated mast cells, and eosinophils was increased in the NEC gut, consistent with the previous studies (19-24). However, the role of adaptive immunity, especially T cells, in NEC has been controversial (25,26). Furthermore, we found that the NEC group was significantly less enriched in adaptive immune cells (naïve B cells, $CD8^+$ T cells, naïve $CD4^+$ T cells, and memory-activated $CD4^+$ T cells) than the Control group.

It is known that levels of mtDNA and mtROS signalling in the cytoplasm are vital factors in innate immunity via the activation of NLRP3 and the secretion of IL-1β (27). Being involved in mitochondrial antigen presentation and immune cell homeostasis, mitophagy indirectly regulates immune cell fate and function (28). Hence, we also established that the hub MRDEGs are closely related to the activation of several immune cells like macrophages, activated mast cells, neutrophils, etc. Among them, HIF-1α and ACSL4 were significantly positively correlated with neutrophils, etc. PCK2 and AIFM1, on the other hand, were significantly positively correlated with M2 macrophages, etc.

A major TF, HIF-1α is associated with oxidative stress and is involved in NEC pathogenesis. Several previous studies have suggested that increased HIF-1α expression is seen in the intestines of both children with NEC and animal models (29,30), and its signaling mediates NEC-associated intestinal microvascular damage (31). Our study also found that the HIF-1α expressions were enhanced in NEC mice intestines. HIF-1α play a critical role in maintaining

intestinal epithelial homeostasis by initiating the mitophagy via activated expression of BCL2/adenovirus E1B 19 kDa protein-interacting protein 3-like (BNIP3L) (32). It has been shown that neutrophils stabilize HIF-1A through the release of mitochondrial ROS via glycolysis, which maintaining mitochondrial membrane potential and cell survival (33). Hence, targeting HIF-1α might be a promising strategy for treating NEC cases by targeting innate immune cells.

Iron uptake-induced upregulation of ACSL4 is required for mitophagy activation and degradation of glutathione peroxidase 4 (GPX4) (34). Consistent with a previous study (35), we observed an elevated ACSL4 expression in NEC mice intestines. Elevated ACSL4 expressions in NEC might regulate the crosstalk between programmed cell death, mitochondrial oxidative stress, and inflammation in various intestinal cells. A study found that inhibition of ACSL4 deficiency is promising for suppressed neutrophil migration in chemical-induced lung injury (36). However, studies on the role of ACSL4 in the pathogenesis of NEC through the regulation of mitophagy and the subsequent innate immune response are lacking and need to be further explored.

PCK2, in addition to mediating gluconeogenesis (37), has been shown to regulate phosphoglycerol synthesis (38). Phosphoglycerol is necessary for producing glycerophospholipids, a major component of biological membranes and therefore precise mitochondrial phospholipid levels are required for normal mitochondrial function (39). In addition, decreased PCK2 expression enhances the abundance of tricarboxylic acid (TCA) cycle intermediates and increases mitochondrial respiration as well as glutathione oxidation. Thus, PCK2 may have a protective role against respiration-induced oxidative stress (40). A study unveils the pivotal role of PCK2 in regulating immunoglobulin A (IgA) antibody-secreting cells' redox balance and antibody production in intestine (41). Regulating the PCK2/AMPK/mTOR signaling pathway can promote M2 macrophage polarization (42). Although most of the existing studies have focused on its function in colitis, this study is the first one to verify the reduced PCK2 expressions in NEC. Further studies are needed to explore the role of PCK2 in NEC cases.

AIFM1 is a mitochondrial flavoprotein involved in the regulation of cysteine-dependent cell death and respiratory chain complex biogenesis. Mitochondrial ROS regulated by AIFM1 influences the generation of $CD8^+$ T cells (43). Our study taps into the fact that AIFM1 expression is decreased in NEC, which may lead to impaired antioxidant expression, increased ROS bursts and oxidative damage to proteins in intestinal cells. In addition, our study also found a positive correlation between PCK2 and $CD8^+$ T cells.

In our study, the expression of MRGs in NEC and their possible interactions with the immune microenvironment were identified for the first time using bioinformatics. HIF-1α, ACSL4, PCK2, and AIFM1 were screened and validated to provide potential molecular targets for in-depth investigation of NEC pathogenesis. There are some limitations in this study. Firstly, the study involved a small sample size of datasets, and more datasets should be included for future analyses. Secondly, the hub genes were only validated in NEC mice and lacked clinical data support. Thirdly, the gestational age difference between the Control and NEC groups in the original dataset (34 *vs.* 28 weeks) may introduce a confounding factor. Due to the limitations of using a publicly available dataset, we were unable to adjust for this difference statistically, as the sample size was already small, and further adjustments would have reduced the number of available samples. This difference in gestational age may lead to inconsistencies in the maturity of mitochondrial development and immune response in intestinal cells, which could impact the susceptibility to NEC. Lastly, additional experiments to validate the regulatory role of MRGs on infiltrating immune cells were lacking. Therefore, the underlying mechanisms of MRGs and their immune infiltration in NEC still need to be further explored both *in vivo* and *in vitro*. Therefore, subsequent studies on NEC pathogenesis will focus on this new direction.

Conclusions

MRGs might induce or inhibit the development of NEC by regulating immune cell infiltration. Targeting *HIF1A*, *ACSL4*, *PCK2*, and *AIFM1* genes might improve the abnormal immune status in further research.

Acknowledgments

The authors thank the contributors to the GEO database for sharing data.

Footnote

Reporting Checklist: The authors have completed the ARRIVE reporting checklist. Available at https://tp.amegroups.com/article/view/10.21037/tp-24-441/rc

Data Sharing Statement: Available at https://tp.amegroups.

com/article/view/10.21037/tp-24-441/dss

Peer Review File: Available at https://tp.amegroups.com/article/view/10.21037/tp-24-441/prf

Funding: This work was supported by grants from the General Program of the National Natural Science Foundation of China (No. 82271741), and Suzhou Gusu Health Talent Plan Project (No. GSWS2022055).

Conflicts of Interest: All authors have completed the ICMJE uniform disclosure form (available at https://tp.amegroups.com/article/view/10.21037/tp-24-441/coif). The authors have no conflicts of interest to declare.

Ethical Statement: The authors are accountable for all aspects of the work in ensuring that questions related to the accuracy or integrity of any part of the work are appropriately investigated and resolved. Animal experiments were performed under a project license (No. SUDA20240108A01) granted by the Ethics Committee of Soochow University, in compliance with the Ethics Committee of Soochow University institutional guidelines for the care and use of animals.

References

1. Qian T, Zhang R, Zhu L, et al. Necrotizing enterocolitis in low birth weight infants in China: Mortality risk factors expressed by birth weight categories. Pediatr Neonatol 2017;58:509-15.
2. Warner BB, Deych E, Zhou Y, et al. Gut bacteria dysbiosis and necrotising enterocolitis in very low birthweight infants: a prospective case-control study. Lancet 2016;387:1928-36.
3. Hackam DJ, Sodhi CP. Bench to bedside - new insights into the pathogenesis of necrotizing enterocolitis. Nat Rev Gastroenterol Hepatol 2022;19:468-79.
4. Han J, Li W, Shi G, et al. Atractylenolide III Improves Mitochondrial Function and Protects Against Ulcerative Colitis by Activating AMPK/SIRT1/PGC-1α. Mediators Inflamm 2022;2022:9129984.
5. Feng YD, Ye W, Tian W, et al. Old targets, new strategy: Apigenin-7-O-β-d-(-6''-p-coumaroyl)-glucopyranoside prevents endothelial ferroptosis and alleviates intestinal ischemia-reperfusion injury through HO-1 and MAO-B inhibition. Free Radic Biol Med 2022;184:74-88.
6. He S, Liu G, Zhu X. Human breast milk-derived exosomes may help maintain intestinal epithelial barrier integrity. Pediatr Res 2021;90:366-72.
7. Dang D, Meng Z, Zhang C, et al. Heme induces intestinal epithelial cell ferroptosis via mitochondrial dysfunction in transfusion-associated necrotizing enterocolitis. FASEB J 2022;36:e22649.
8. Zhang Q, Raoof M, Chen Y, et al. Circulating mitochondrial DAMPs cause inflammatory responses to injury. Nature 2010;464:104-7.
9. Lu Y, Li Z, Zhang S, et al. Cellular mitophagy: Mechanism, roles in diseases and small molecule pharmacological regulation. Theranostics 2023;13:736-66.
10. Zani A, Zani-Ruttenstock E, Peyvandi F, et al. A spectrum of intestinal injury models in neonatal mice. Pediatr Surg Int 2016;32:65-70.
11. Zhang Y, Yan M, Yue Y, et al. Hypoxia-Inducible Factor-1α Modulates the Toll-Like Receptor 4/Nuclear Factor Kappa B Signaling Pathway in Experimental Necrotizing Enterocolitis. Mediators Inflamm 2024;2024:4811500.
12. Caplan MS, Hedlund E, Hill N, et al. The role of endogenous nitric oxide and platelet-activating factor in hypoxia-induced intestinal injury in rats. Gastroenterology 1994;106:346-52.
13. Haberman Y, Karns R, Dexheimer PJ, et al. Ulcerative colitis mucosal transcriptomes reveal mitochondriopathy and personalized mechanisms underlying disease severity and treatment response. Nat Commun 2019;10:38.
14. Peña-Cearra A, Castelo J, Lavín JL, et al. Mitochondrial dysfunction-associated microbiota establishes a transmissible refractory response to anti-TNF therapy during ulcerative colitis. Gut Microbes 2023;15:2266626.
15. Zhang YF, Fan MY, Bai QR, et al. Precision therapy for ulcerative colitis: insights from mitochondrial dysfunction interacting with the immune microenvironment. Front Immunol 2024;15:1396221.
16. Baregamian N, Song J, Papaconstantinou J, et al. Intestinal mitochondrial apoptotic signaling is activated during oxidative stress. Pediatr Surg Int 2011;27:871-7.

17. Bindi E, Li B, Zhou H, et al. Mitochondrial DNA: A Biomarker of Disease Severity in Necrotizing Enterocolitis. Eur J Pediatr Surg 2020;30:85-9.
18. He-Yang J, Zhang W, Liu J, et al. Human breast milk oligosaccharides attenuate necrotizing enterocolitis in rats by suppressing mast cell accumulation, DPPI activity and TLR4 expression in ileum tissue, and regulating mitochondrial damage of Caco-2 cells. Int Immunopharmacol 2020;88:106881.
19. Liu Y, Zhou J, Chen B, et al. High-dimensional mass cytometry reveals systemic and local immune signatures in necrotizing enterocolitis. Front Immunol 2023;14:1292987.
20. Fu H, Zhang P, Zhao XD, et al. Interfering with Rac1-activation during neonatal monocyte-macrophage differentiation influences the inflammatory responses of M1 macrophages. Cell Death Dis 2023;14:619.
21. Olaloye OO, Liu P, Toothaker JM, et al. CD16+CD163+ monocytes traffic to sites of inflammation during necrotizing enterocolitis in premature infants. J Exp Med 2021;218:e20200344.
22. Liu Q, Gao K, Ding X, et al. NAMPT inhibition relieves intestinal inflammation by regulating macrophage activation in experimental necrotizing enterocolitis. Biomed Pharmacother 2023;165:115012.
23. Zhang W, He-Yang J, Zhuang W, et al. Causative role of mast cell and mast cell-regulatory function of disialyllacto-N-tetraose in necrotizing enterocolitis. Int Immunopharmacol 2021;96:107597.
24. Wahidi LS, Sherman J, Miller MM, et al. Early Persistent Blood Eosinophilia in Necrotizing Enterocolitis Is a Predictor of Late Complications. Neonatology 2015;108:137-42.
25. Luo S, Zeng Y, Chen B, et al. Vitamin E and GPX4 cooperatively protect treg cells from ferroptosis and alleviate intestinal inflammatory damage in necrotizing enterocolitis. Redox Biol 2024;75:103303.
26. Egozi A, Olaloye O, Werner L, et al. Single-cell atlas of the human neonatal small intestine affected by necrotizing enterocolitis. PLoS Biol 2023;21:e3002124.
27. Nakahira K, Haspel JA, Rathinam VA, et al. Autophagy proteins regulate innate immune responses by inhibiting the release of mitochondrial DNA mediated by the NALP3 inflammasome. Nat Immunol 2011;12:222-30.
28. Song Y, Zhou Y, Zhou X. The role of mitophagy in innate immune responses triggered by mitochondrial stress. Cell Commun Signal 2020;18:186.
29. Bai M, Lu C, An L, et al. SIRT1 relieves Necrotizing Enterocolitis through inactivation of Hypoxia-inducible factor (HIF)-1a. Cell Cycle 2020;19:2018-27.
30. Yuan Y, Ding D, Zhang N, et al. TNF-α induces autophagy through ERK1/2 pathway to regulate apoptosis in neonatal necrotizing enterocolitis model cells IEC-6. Cell Cycle 2018;17:1390-402.
31. Zhang Y, Zhang X, Tian B, et al. Hypoxia-Inducible Factor 1α Stability Modified by Glutaredoxin-1 in Necrotizing Enterocolitis. J Surg Res 2022;280:429-39.
32. Vincent G, Novak EA, Siow VS, et al. Nix-Mediated Mitophagy Modulates Mitochondrial Damage During Intestinal Inflammation. Antioxid Redox Signal 2020;33:1-19.
33. Willson JA, Arienti S, Sadiku P, et al. Neutrophil HIF-1α stabilization is augmented by mitochondrial ROS produced via the glycerol 3-phosphate shuttle. Blood 2022;139:281-6.
34. Zhang L, Wang F, Li D, et al. Transferrin receptor-mediated reactive oxygen species promotes ferroptosis of KGN cells via regulating NADPH oxidase 1/PTEN induced kinase 1/acyl-CoA synthetase long chain family member 4 signaling. Bioengineered 2021;12:4983-94.
35. Dang D, Zhang C, Meng Z, et al. Integrative analysis links ferroptosis to necrotizing enterocolitis and reveals the role of ACSL4 in immune disorders. iScience 2022;25:105406.
36. Tomitsuka Y, Imaeda H, Ito H, et al. Gene deletion of long-chain acyl-CoA synthetase 4 attenuates xenobiotic chemical-induced lung injury via the suppression of lipid peroxidation. Redox Biol 2023;66:102850.
37. Grasmann G, Smolle E, Olschewski H, et al. Gluconeogenesis in cancer cells - Repurposing of a starvation-induced metabolic pathway? Biochim Biophys Acta Rev Cancer 2019;1872:24-36.
38. Leithner K, Triebl A, Trötzmüller M, et al. The glycerol backbone of phospholipids derives from noncarbohydrate precursors in starved lung cancer cells. Proc Natl Acad Sci U S A 2018;115:6225-30.
39. Tasseva G, Bai HD, Davidescu M, et al. Phosphatidylethanolamine deficiency in Mammalian mitochondria impairs oxidative phosphorylation and alters mitochondrial morphology. J Biol Chem 2013;288:4158-73.
40. Bluemel G, Planque M, Madreiter-Sokolowski CT, et al. PCK2 opposes mitochondrial respiration and maintains the redox balance in starved lung cancer cells. Free Radic Biol Med 2021;176:34-45.
41. Duan KL, Wang TX, You JW, et al. PCK2 maintains intestinal homeostasis and prevents colitis by protecting

antibody-secreting cells from oxidative stress. Immunology 2024;173:339-59.
42. Tang D, Han B, He C, et al. Electrospun Poly-l-Lactic Acid Membranes Promote M2 Macrophage Polarization by Regulating the PCK2/AMPK/mTOR Signaling Pathway. Adv Healthc Mater 2024;13:e2400481.
43. Bertaux A, Cabon L, Brunelle-Navas MN, et al. Mitochondrial OXPHOS influences immune cell fate: lessons from hematopoietic AIF-deficient and NDUFS4-deficient mouse models. Cell Death Dis 2018;9:581.

Cite this article as: Jin X, Sun W, Li Y, Zhu X. Mitophagy and immune cell interaction: insights into pathogenesis and potential targets for necrotizing enterocolitis. Transl Pediatr 2025;14(2):171-186. doi: 10.21037/tp-24-441